Electronic Supplementary Material (ESI) for Physical Chemistry Chemical Physics.

Electronic Supplementary Information for

Wavepacket dynamical study of H atom tunneling in catecholate monoanion: Role of intermode couplings and energy flow

Debabrata Bhattacharyya and Sai G. Ramesh

Department of Inorganic and Physical Chemistry, Indian Institute of Science, Bangalore 560012, India

TABLE S1. **Parameters for 1D Hamiltonians.** For each mode Q_j, a 1D potential cut $V_{ad}(Q_j;\boldsymbol{Q}_o)$ is chosen to solve for eigenstates, where $\boldsymbol{Q}_o$ represents the fixed values of other modes. We have chosen only one mode (Q_{10} for $j=1$ and Q_1 for all other modes) to be non-zero in $\boldsymbol{Q}_o$. For the chosen cut for each Q_j, the location of the potential minimum $Q_{j,min}$ is tabulated, along with the potential energy $E_{j,min}$ and local frequency $\tilde{\nu}_{j,min}$ (in cm^{-1}) at this point.

Q_j	Q_{fixed}	(Value)	$Q_{j,min}$	$E_{j,min}$	$\tilde{\nu}_{j,min}$
Q_1	Q_{10}	(+2.02)	−2.02	−930.4	4966.5
Q_7	Q_1	(−1.26)	0.06	−536.5	597.1
Q_{10}	Q_1	(−2.02)	1.68	−936.2	823.7
Q_{13}	Q_1	(−1.26)	−0.06	−536.9	832.0
Q_{27}	Q_1	(−1.26)	0.08	−540.1	1623.9
Q_{29}	Q_1	(−1.58)	0.40	−631.7	2347.5

TABLE S2. **Eigenvalues of 1D Hamiltonians.** These are obtained from the solutions of the 1D Hamiltonians in primitive basis functions (see Phys. Chem. Chem. Phys. 24, 10887 (2022)). For mode Q_1, the eigenkets are additionally denoted by their parity.

Q_j	$\lvert j_l\rangle$	$\varepsilon_l^{(j)}$	Q_j	$\lvert j_l\rangle$	$\varepsilon_l^{(j)}$
	$\lvert 1_0^+\rangle$	186.6		$\lvert 7_0\rangle$	−255.6
	$\lvert 1_0^-\rangle$	246.7		$\lvert 7_1\rangle$	302.7
	$\lvert 1_1^+\rangle$	1680.7	Q_7	$\lvert 7_2\rangle$	859.0
	$\lvert 1_1^-\rangle$	2483.3		$\lvert 7_3\rangle$	1416.8
Q_1	$\lvert 1_2^+\rangle$	3702.5		$\lvert 7_4\rangle$	1975.0
	$\lvert 1_2^-\rangle$	5130.0			
	$\lvert 1_3^+\rangle$	6701.5			
	$\lvert 1_3^-\rangle$	8428.1		$\lvert 13_0\rangle$	−137.1
				$\lvert 13_1\rangle$	658.2
	$\lvert 10_0\rangle$	−583.8	Q_{13}	$\lvert 13_2\rangle$	1450.6
	$\lvert 10_1\rangle$	135.5		$\lvert 13_3\rangle$	2243.5
Q_{10}	$\lvert 10_2\rangle$	857.0		$\lvert 13_4\rangle$	3036.1
	$\lvert 10_3\rangle$	1576.2			
	$\lvert 10_4\rangle$	2284.4		$\lvert 27_0\rangle$	254.4
	$\lvert 10_5\rangle$	2978.2	Q_{27}	$\lvert 27_1\rangle$	1840.3
				$\lvert 27_2\rangle$	3425.7
	$\lvert 29_0\rangle$	468.3			
Q_{29}	$\lvert 29_1\rangle$	2620.2			
	$\lvert 29_2\rangle$	4665.3			

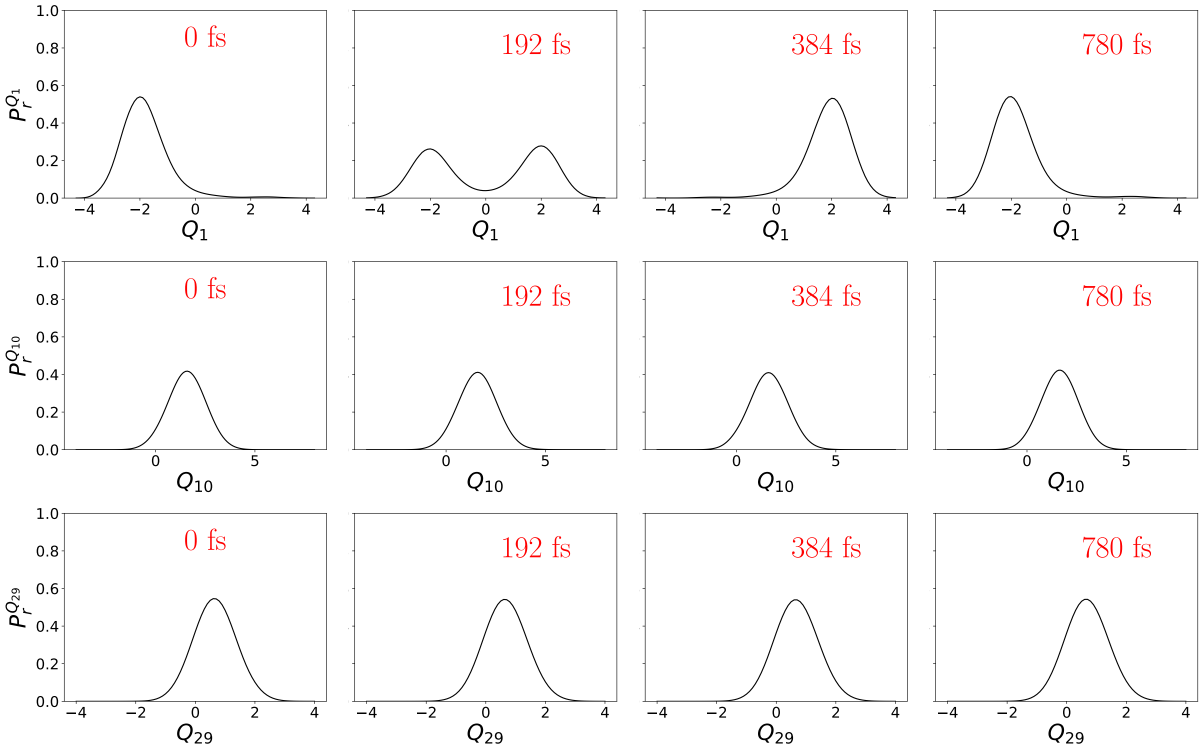

FIG. S1. **Tunneling from linear combination of eigenstates.** Reduced probability densities along Q_1, Q_{10}, and Q_{29} are given for 3D dynamics carried out for the linear combination of the ground tunneling split pair of eigenfunctions. A coherent oscillation of the wavepacket is observed along Q_1, while it is essentially stationary along the other two modes.

TABLE S3. **Composition of direct product states used for wavepacket analyses.** Given in the table are the maximum excitations (number of quanta) in each mode that are used to construct left and right direct product states, which in turn are used for the expansion of the evolving wavepackets. For Q_1, both $\pm$ state pairs are included for each excitation.

Mode space	$\vec{v}_{max}$	Mode space	$\vec{v}_{max}$
Q_1-Q_{10}	(4, 13)	Q_1-Q_7	(4, 5)
Q_1-Q_{29}	(4, 4)	Q_1-Q_{13}	(4, 5)
Q_1-Q_{10}-Q_{29}	(6, 7, 4)	Q_1-Q_{27}	(4, 4)

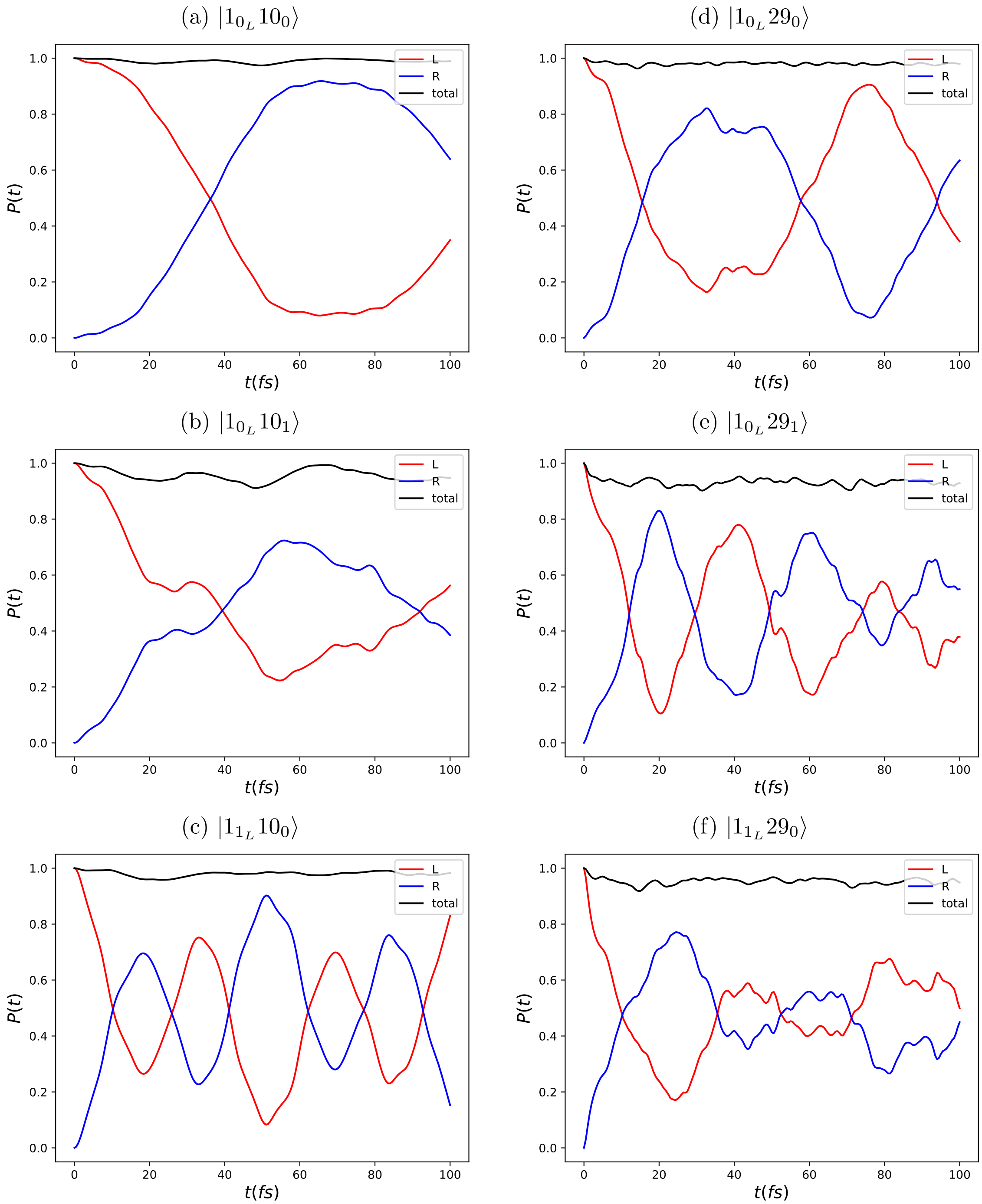

FIG. S2. **Cumulative projected populations for selected initial conditions.** For all Q_1-Q_{10} initial states (a-c), the populations in direct products $|1_{l_{L/R}}10_m\rangle$ summed up to $0 \leq l \leq 2$ and $0 \leq m \leq 5$ are shown. Similarly, for all Q_1-Q_{29} initial states (d-f), the populations in direct products $|1_{l_{L/R}}29_n\rangle$ summed up to $0 \leq l \leq 3$ and $0 \leq n \leq 2$ are shown. The red and blue curves are the total left and right-well populations, while the black curves are the sum of the two. Including more quanta in the summations provides minor changes to the cumulative probabilities. In this sense, the set of direct products used for the plots may be used for a qualitative and (nearly) quantitative analysis. However, we emphasize that the full set of direct products as given in table S3 was used for all the numerical analysis in this work, which includes several more direct products.

Dynamics in 2D Q_1-Q_7, Q_1-Q_{13} and Q_1-Q_{27} spaces

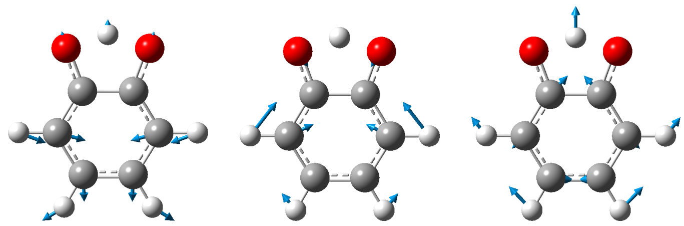

(a) Q_7 (b) Q_{13} (c) Q_{27}

FIG. S3. Minimally coupled modes of CM

In our previous study (Phys. Chem. Chem. Phys. 24, 10887 (2022)) we noted that modes Q_7, Q_{13} and Q_{27} are minimally coupled to the tunneling mode Q_1. The modes are shown in Figure S3. Consequently, the dynamics in 2D spaces involving these modes are expected to be simple in comparison to those for Q_1-Q_{10} and Q_1-Q_{29}. Figure S4 shows $P_{tun}(t)$ for the different direct product initial states, viz. $|1_{0_L} y_0\rangle$, $|1_{0_L} y_1\rangle$, and $|1_{1_L} y_0\rangle$ where $y = 7$, 13, or 27. The plots for all three modes are very similar, suggesting that the dynamics is largely independent of the identity of the minimally coupled mode. For both zero or one quantum of excitation in Q_y, the first passage times ($\sim$20 fs) are essentially the same. This suggests insentivity of the dynamics, at least at short times, to Q_y excitation. However, the dynamics at later times is a slightly different for Q_{27} compared to Q_7 and Q_{13}. With one quantum of excitation in Q_1, the tunneling is expectedly faster and is also very similar for all Q_y.

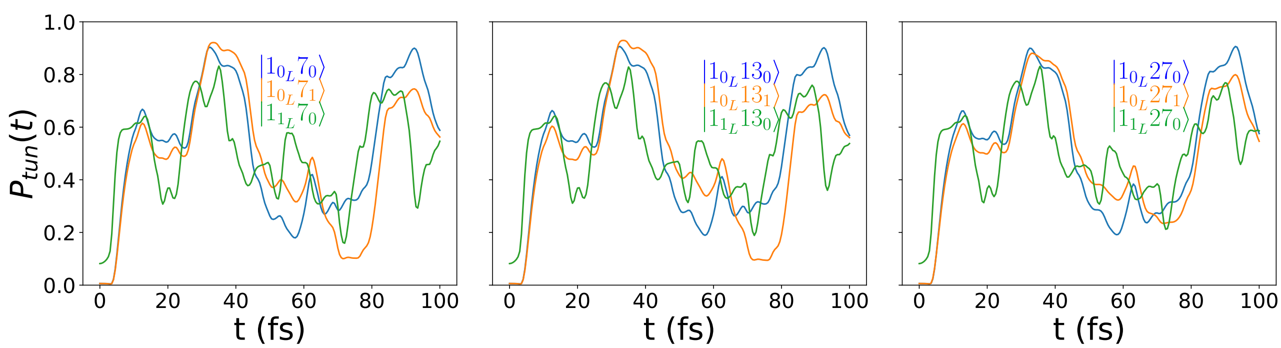

FIG. S4. Tunneling probabilities in the Q_1-Q_7, Q_1-Q_{13}, and Q_1-Q_{27} spaces for various initial states.

Figure S5 shows the mode energies as a function of time for various initial wavepackets. The $\langle E^{(y)}\rangle$ are practically constant for Q_7 and Q_{13}, and show a slow variation for Q_{27} over the length of the dynamics for the indicated initial states. These indicate essentially negligible or little energy flow between Q_1 and Q_y in all cases. It is evident that $\langle E^{(1)}\rangle$ shows an oscillatory trend. As the total energy is constant, the remainder of the energy is in $\langle E_{res}\rangle$ whose trend (not shown) is an an inverted version of $\langle E^{(1)}\rangle$. The non-constancy of $\langle E^{(1)}\rangle$ is due to the choice of Hamiltonian partitioning described in the manuscript.

Figure S6 shows the average positions of the modes as a function of time for various initial states. The $\langle Q_y\rangle$ is also almost constant for Q_7 and Q_{13}, while Q_{27} shows an notable oscillatory trend.

The projected population for dynamics from various initial states is given in S7. Since Q_1-Q_7 and Q_1-Q_{13} give almost identical pictures of the dynamics, only plots for selected initial states in Q_1-Q_7 and Q_1-Q_{27} spaces are shown. The plots indicate that, for a given initial state, the populations are contained within the same $|y_0\rangle$ or $|y_1\rangle$ state. All the significant direct products differ only in the number of quanta in Q_1. This is corroborated by systematic analysis of the cumulative projected populations, where contributions from other states of Q_y negligibly change the sum.

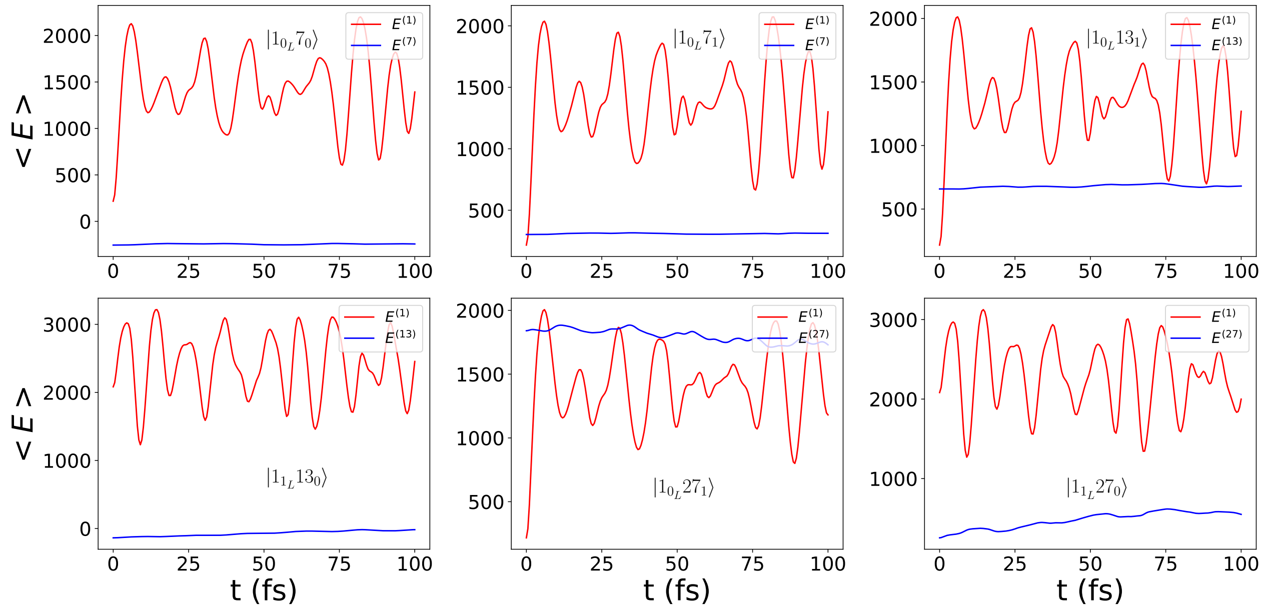

FIG. S5. Time-evolution of mode energies in cm^{-1} for various initial wavepackets in the Q_1-Q_7, Q_1-Q_{13}, and Q_1-Q_{27} spaces.

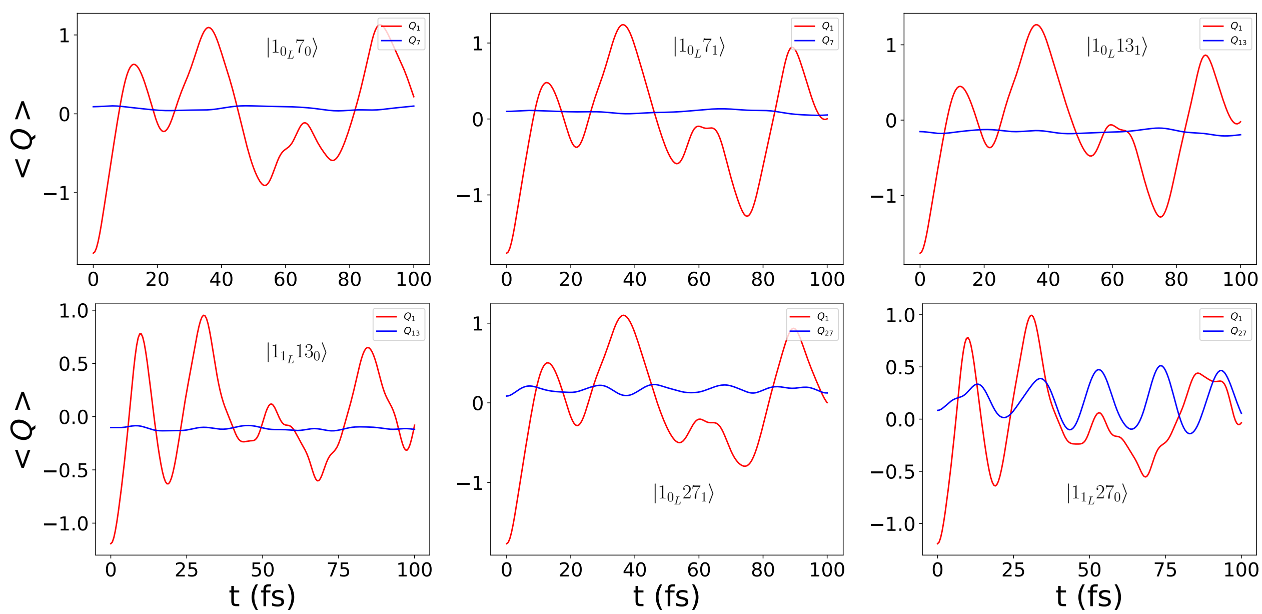

FIG. S6. Time-evolution of position expectation values of Q_1 and Q_y, $y = 7$, 13, 27, for various initial conditions.

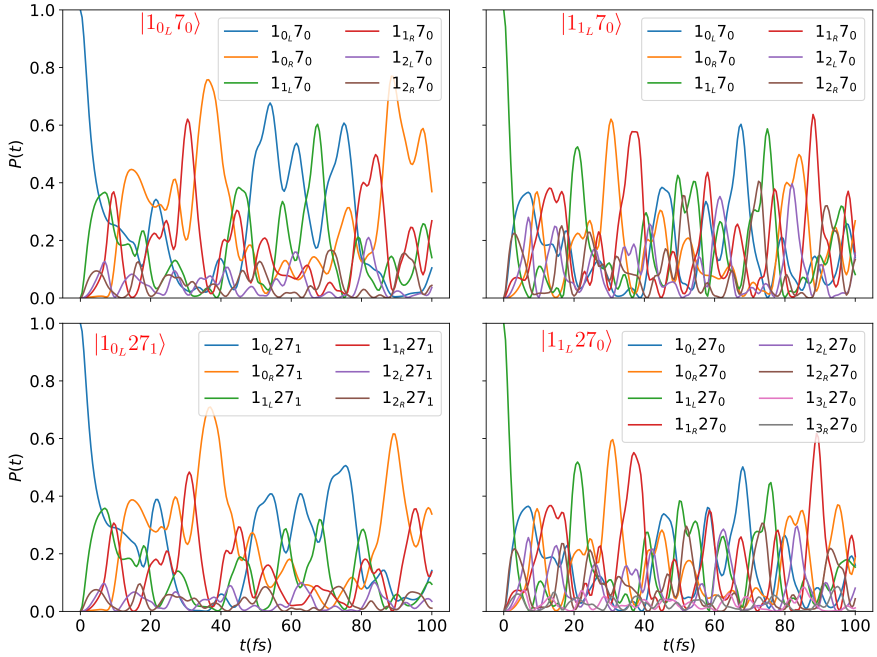

FIG. S7. Projected populations in various direct product states for the $|1_{0_L}7_0\rangle$, $|1_{1_L}7_0\rangle$, $|1_{0_L}27_1\rangle$, and $|1_{1_L}27_0\rangle$ initial states.

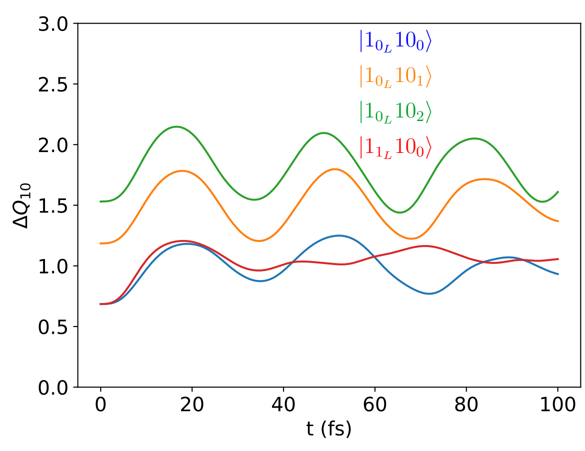

FIG. S8. Complementary to the plot of $\langle Q_{10}\rangle$ shown in Fig. 4, here the widths of the evolving packets along Q_{10} are shown for all 2D initial conditions in the Q_1-Q_{10} space. This is calculated as $\Delta Q_{10} = \sqrt{\langle Q_{10}^2\rangle - \langle Q_{10}\rangle^2}$. Note that the widths increase with Q_{10} excitation as the initial packet is already more spread.

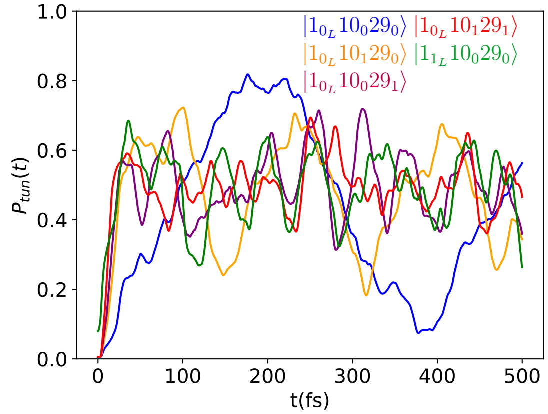

FIG. S9. Variation of tunneling probability in the Q_1-Q_{10}-Q_{29} space for various initial states. An abbreviated version of this plot with the time axis limited to 200 fs is given in Fig. 8.

(a)

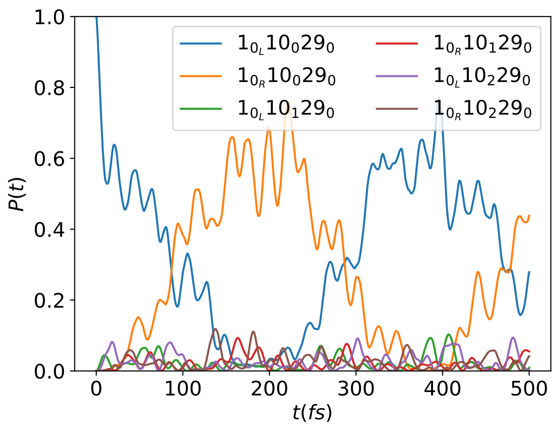

(b)

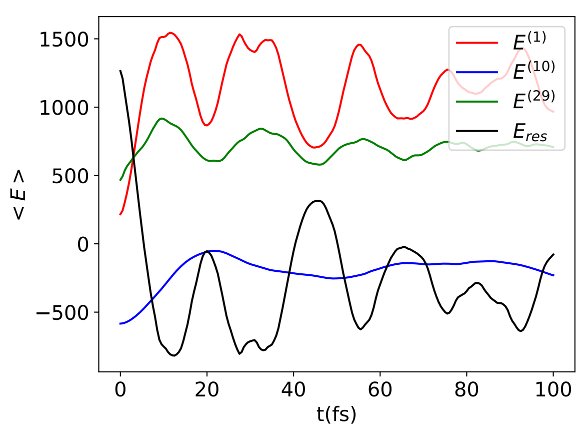

FIG. S10. (a) Projected population and (b) mode energy variation (in cm^{-1}) for dynamics from the $|1_{0_L}10_0 29_0\rangle$ initial state.